Convective dispersion of particles in a segmented flow

Wafa Bouhlel,[1,2] S. Danial Naghib,[1] Jérôme Bibette,[1] and Nicolas Bremond [1,*]

[1]*Institute of Chemistry, Biology and Innovation (CBI) UMR8231, CNRS, ESPCI Paris, PSL* Research University, 10 rue Vauquelin, F-75005 Paris, France*
[2]*Sorbonne University, 4 place Jussieu, F-75005 Paris, France*

Convective dispersion of solutes is inherent to flow in channels because of the nonuniformity of the velocity profile. When diffusion is negligible, for large particles for example, the trajectory of particles can be solely described by a kinematic approach. Here, we investigate such a phenomenon for micrometer-size beads flowing in a circular pipe. We show that the presence of large bubbles, namely in the case of a segmented flow, either prevents the convective dispersion or leads to the accumulation of particles at the rear of the bubble moving in front. The destabilization of the initially homogeneous suspension occurs when liquid inertia comes into play. Indeed, for moderate Reynolds number of the particles, particles move away from the wall, thus exploring different flow lines that finally impact the axial dispersion features. Moreover, since the bubbles impose an axial boundary condition of the mean velocity, a net flux of particles directed along the flow direction is built up above a critical particle Reynolds number. This work is motivated by the understanding of the flow behavior of biological samples, and especially in the context of cell encapsulation.

I. INTRODUCTION

Flow of particle suspensions in channels is encountered in many situations, from natural systems, such as blood flow, to engineering processes, such as in the food, pharmaceutical, or biotechnology industries. A well-studied phenomenon is the spatial redistribution of particles in confined flows due to lateral migration of particles [1,2]. For moderate Reynolds numbers, particles tend to focus on specific regions in a channel flow [3]. This behavior has been recently exploited in microfluidic systems for cell ordering and sorting applications [4]. This strategy, named inertial microfluidics and where particles tend to self-organize in a train [5], is also relevant for cell encapsulation in emulsion droplets in order to overcome the otherwise inherent statistical distribution of an encapsulated cell number at low concentrations [6]. For other techniques of cell encapsulation relying on liquid atomization [7,8], where liquid inertia is needed for creating compound liquid jets [9], the flow features of suspension of cells have an impact on the encapsulation process. Moreover, for such an encapsulation strategy, the ability to manipulate a relatively small amount of biological samples, i.e., a few ml, is a key feature when handling precious samples. Since the process is a continuous one, which involves flow rates of the order of 100 mL/h, samples to be encapsulated should be injected in a sequential way into the main flow of the continuous phase, such as for chromatography analysis. Convective dispersion that leads to a longitudinal variation of solute concentration is then inevitably in action [10].

---

*nicolas.bremond@espci.fr

Here, we investigate the convective dispersion features of a suspension of neutrally buoyant microparticles flowing in a pipe at moderate Reynolds numbers and volume fractions. Adding long bubbles that bound the sample can, in principle, limit this concentration heterogeneity, as is done in flow chemistry [11], for making particles [12] or by using particles as catalysts [13]. We thus study the features of suspensions in a segmented flow and observe a striking behavior when liquid inertia comes into play.

II. MATERIALS AND METHODS

Particles of different sizes and types are used. The first ones are carbon nanotubes (CNT) labeled Graphistrengh C100 (Arkema). As previously described [14], carbon nanotubes are dispersed in water at a concentration of 0.2 wt% by sonication in the presence of 0.1 wt% surfactants (Brij 35, Sigma Aldrich). The corresponding mean hydrodynamic diameter is 190 nm as measured by light scattering (Nanosizer, Malvern). The second type of particles consists of is polystyrene (PS) beads (Dynoseeds TS 20 and TS 40, Microbeads). The average diameters d, measured by light diffraction (Mastersizer 3000, Malvern), are 20.5 and 40 μm with a coefficient of variation of 15% and 11%, respectively. They are also dispersed in water with the help of surfactants, i.e., Tween 20 and sodium dodecyl sulfate (SDS) (Sigma Aldrich). In addition, the density of the aqueous phase is matched with the bead density, which is 1.05 kg/m^3, by adding a non-ionic molecule (Nycodenz, Proteogneix). Hydrosoluble polymers, poly(ethylene) glycol (PEG) (PEG 3000 and PEG 20000, Sigma Aldrich), are used for increasing the continuous phase fluid viscosity. Viscosity of the continuous phase is measured with a rheometer (ARG2, TA Instruments) in a cone-plane geometry and equal to 1.2 mPa s, 4.4 mPa s (with PEG 3000 at 10 wt%), and 8.8 mPa s (with PEG 20000 at 7 wt%). A stock suspension of beads at a volume fraction of 0.2 is prepared by adding 0.1 wt% of Tween 20, or 0.2 wt% of SDS and 10 wt% of Nycodenz. We note that SDS is preferred as its adsorption kinetics at the interfaces is faster, thus facilitating a rapid and complete wetting of the continuous phase on the tube's wall and also ensuring a better stabilization of the lubricating film. The corresponding surface tension γ at equilibrium is about 35 mN/m for all solutions. When PEG is used, the Nycodenz concentration is adjusted. All solutions are prepared using ultrapure water (Milli-Q).

The experimental setup is sketched in Fig. 1(a). The continuous phase is injected with a syringe pump (PhD Ultra, Harvard Apparatus) through a teflon tube having an inner diameter of 0.81 or 1.05 mm. The fluid either flows straight to the measurement area or passes through a parallel circuit where the sample is loaded. The direction is controlled by switching the closing state of two pinch valves (Bio-Chem Fluidics) located on each arm of the loop. Since Teflon is a ductile material, a 2-cm-long elastic tube made of tygon is placed at the location of each pinch valve. The sample is loaded in a Teflon tube having a length $L_s = 40$ cm, or otherwise noted, and inserted into the circuit via two T junctions. This latter arrangement is equipped with manual on-off valves (Upchurch, Idex) to avoid fluid leakage when inserting the sample. Long air bubbles can be introduced in the main circuit just prior to the on-off valves and before closing them. This allows one to bound the sample with bubbles having a length larger than the tube diameter. The Teflon tube after the second T junction is connected via a flexible tube to a circular cross-section glass capillary having an inner diameter of 0.78 mm (Vitrocom). Having parallel flow lines allows one to well set the fluidic system before injecting the sample, such as in liquid chromatography analysis. We note that since the tube at the measurement location has a diameter smaller than the tube where the fluid is mostly flowing, the recording time is then multiplied by the square of the diameter ratio when compared to the theoretical prediction in order to respect mass conservation. The capillary is inserted in a square glass capillary (Vitrocom) filled with glycerol for limiting optical distortion introduced by the round capillary. The capillaries are glued on a glass plate and set on a transmitted light microscope (DMI3000, Leica). An objective with a 10x magnification is coupled to a camera (Fastcam 1024-PCI, Photron). Examples of the images recorded during experiments with both suspensions are shown in Figs. 1(b) and 1(c). The system is not free of optical aberrations and the concentration of particles is determined by measuring the transmitted light along the axis of the capillary averaged
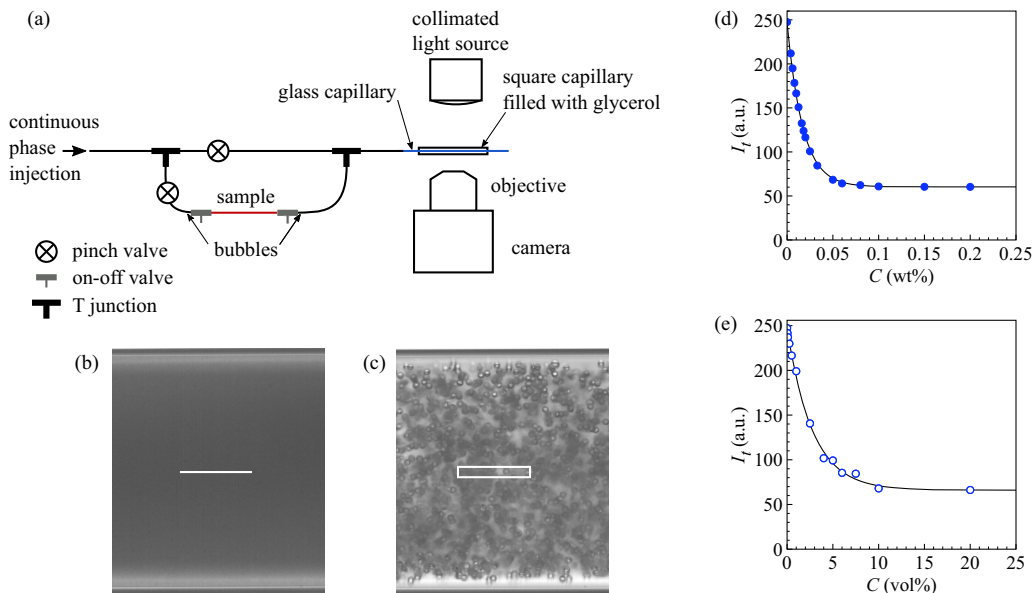
FIG. 1. (a) Schematics of the experimental setup. (b) Snapshot of CNT suspension flowing in the glass capillary. The white line shows the area from which the average transmitted light I_t is evaluated. (c) Snapshot of PS beads suspension flowing in the glass capillary. The white rectangle delimits the area from which I_t is measured. The diameter of the capillary is 0.78 mm. (d) Calibration curve of the CNT suspension. (e) Calibration curve of the PS beads suspension ($d = 20\,\mu$m). The continuous lines represent Eq. (1) from which the attenuation coefficient ε is estimated.

along a single pixel line of 100 pixels for CNT suspensions and within a rectangular box having the same length and a width of 14 pixels, about a bead diameter, in the case of the suspension of beads. The calibration curves for CNT and micrometer beads, obtained by averaging the transmitted light over 500 images for various particles concentrations, are reported in Figs. 1(d) and 1(e), respectively. The transmitted light I_t follows a Beer-Lambert law,

$$I_t = (I_0 - I_\infty)e^{-\varepsilon C} + I_\infty, \tag{1}$$

where ε is an attenuation coefficient, I_0 is the transmitted light without any particles, and I_∞ is the transmitted light when the concentration C of particles tends to infinity. Here, C is either a weight percentage of the CNT or a volume percentage of the PS beads. ε is the only fit parameter, I_0 and I_∞ being directly deduced from the intensity measurements. The attenuation coefficient is equal to 59 per wt% for CNT and to 0.36 per vol% for PS beads.

III. RESULTS AND DISCUSSION

A. Theory of convective dispersion

The dispersion of solutes in a Poiseuille flow was first described by Taylor [10] and later on generalized by Aris [15]. When the diffusion of the solutes or particles is negligible, i.e., for $L/a \ll$ Pe$/3.8^2$ where Pe $= aU/D$ is the Péclet number, L the tube length, a the lateral channel size, U the mean solvent velocity, and D the diffusion coefficient of the particles in the solvent, the convective dispersion features are solely ruled by kinematics (Fig. 2). Here, the smallest particle size along with the smallest flow rate give a minimal Péclet number of the order of 10^6 and the largest value of L/a is about 2.5×10^3. Therefore, diffusion of particles does not have time to take place. For a cylindrical
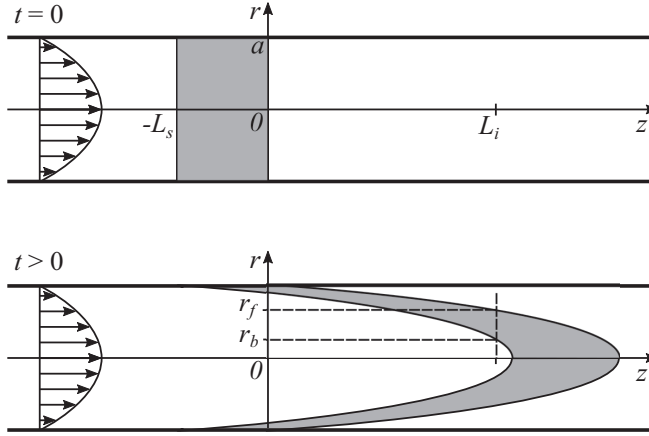
FIG. 2. Schematics illustrating a purely convective dispersion of a solution or suspension subjected to a Poiseuille flow.

geometry, the velocity profile is $u = u_m(1 - r^2/a^2)$, where u_m is the maximal velocity reached at the center of the channel of radius a and r is the radial coordinate. A particle initially located at $\{z_0, r_0\}$ is then advected at a velocity $u(r_0)$. Its longitudinal location z at time t is thus simply $z = z_0 + u_m(1 - r_0^2/a^2)t$. Let us consider a volume of fluid initially contained between $z = -L_s$ and $z = 0$ as sketched in Fig. 2 and named the "sample." The fluid fraction ϕ occupied by the sample in a cross section of the channel taken at a distance $z = L_i$ is then determined by the radial locations of the front interface of the sample $r_f(L_i, t)$ and the back one $r_b(L_i + L_s, t)$. Indeed, ϕ is equal to $(r_f/a)^2 - (r_b/a)^2$ for a cylindrical geometry and to $r_f/a - r_b/a$ for a planar one. Since optical deformation introduced by the curvature of the glass capillary of the present experimental set-up is not completely corrected on the whole cross section with the square capillary, the particle concentration is measured on the tube's axis. In that case, the volume fraction estimate is similar to a planar case and is given by

$$t < \frac{L_i}{u_m}, \qquad \phi = 0,$$

$$\frac{L_i}{u_m} \leqslant t < \frac{L_i + L_s}{u_m}, \qquad \phi = \left(1 - \frac{L_i}{u_m t}\right)^{1/2}, \tag{2}$$

$$\frac{L_i + L_s}{u_m} \leqslant t, \qquad \phi = \left(1 - \frac{L_i}{u_m t}\right)^{1/2} - \left(1 - \frac{L_i + L_s}{u_m t}\right)^{1/2}.$$

Since the value of ϕ is estimated by turbidimetry, i.e., linked to the loss of intensity of transmitted light due to the light scattered by the particles, we assumed that the light attenuation measured during a convective dispersion experiment corresponds to a dispersion having a particle concentration equal to ϕC_0, where C_0 is the particle concentration of the loaded sample. As discussed in Sec. II, the light transmitted through homogeneous samples of various compositions follows a Beer-Lambert law [Eq. (1)] for both particles under study [Figs. 1(d) and 1(e)].

B. Convective dispersion of nanoparticles

The convective dispersion of nanometer-size particles is first reported. A suspension of carbon nanotubes at a concentration of 0.06 wt% is initially injected at a flow rate of 100 mL/h. The time evolution of the CNT concentration measured at a distance L_i from the downstream front of the injected sample equal to 10 cm is reported in Fig. 3(a). The time evolution predicted by Eq. (2)
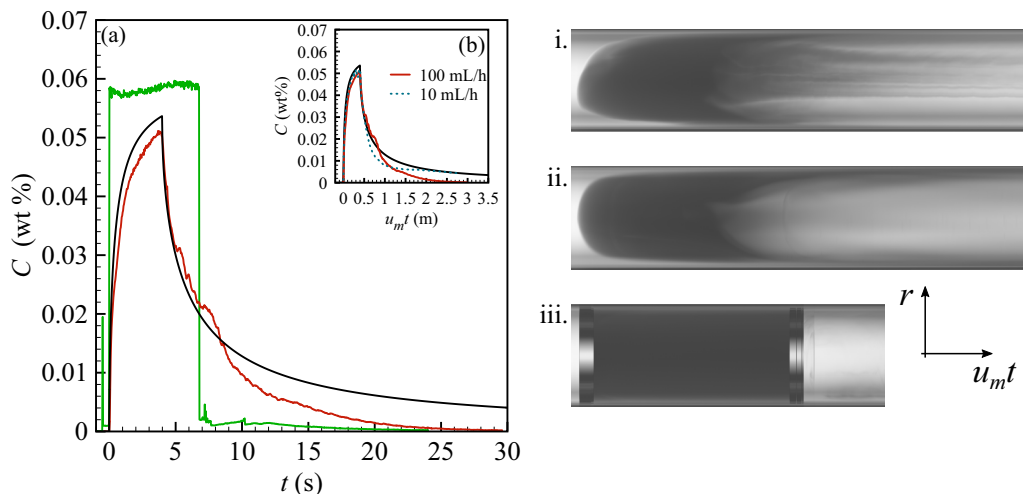
FIG. 3. (a) Time evolution of the concentration of a carbon nanotube suspension undergoing a convective dispersion at a flow rate of 100 mL/h in a capillary having a radius of 405 μm (red curve) along with the evolution predicted by Eq. (2) (black curve) with $C = C_0\phi$. The concentration is measured at a distance L_i equal to 10 cm. The axial dispersion is almost canceled out by adding a large bubble at each end of the sample (green curve). (b) Dispersion curves for two different flow rates and the one predicted by Eq. (2). The time is multiplied by the maximum velocity u_m. Corresponding spatiotemporal diagrams built along the transverse plane of the capillary for (i) $q = 100$ mL/h, (ii) $q = 10$ mL/h, and when bubbles are present at (iii) $q = 100$ mL/h. Time is also multiplied by u_m.

is also shown. The concentration first rises up to about 0.05 wt% and then decreases when the back interface reaches the measurement point. There is a rather good agreement between theory and experiment up to the first 8 s, but then the amount of particles is observed to drop down much faster than predicted. The corresponding spatiotemporal diagram built along the transverse plane of the capillary is shown in Fig. 3(i). Wavy streaks are observed when the CNT concentration starts to decrease. This feature might be linked to the turn at 90° at the T junction located prior to the detection area. The channel Reynolds number, $\text{Re}_c = 2au_m/\nu$, where ν is the kinematic viscosity of the aqueous phase, is equal to 76, secondary flow, or Dean flow, in the transverse direction due to centrifugal force which is susceptible to occur [16]. A more homogeneous concentration field is indeed recovered for a flow rate, and thus a Reynolds number, that is ten times lower [Fig. 3(ii)]. The time evolution of the concentration is then better predicted by a purely convective dispersion mechanism, as shown in Fig. 3(b). We note that since flat initial interfaces between two miscible liquids are difficult to experimentally achieve, corrugations of the sample interfaces inevitably lead to concentration inhomogeneities in the transverse direction, which is evident in Fig. 3(i) after the concentration peak.

Bubbles having a length larger than the tube diameter can be introduced in order to compartmentalize the sample, like in segmented flow chemistry [11]. The corresponding time evolution of the concentration, measured for the largest flow rate, is shown in Fig. 3(a) (green curve) and Fig. 3(iii). The concentration is almost constant between the bubbles, starting with a value of about 0.058 wt% and reaching 0.06 wt% at the front of the second bubble. We also note traces of CNT behind the later bubble. Here, the flow velocity is such that there exists a lubricating water film between the bubbles and the tube wall. The bubbles are then moving at a velocity slightly larger than the average liquid velocity [17]. As a consequence, the continuous phase thus dilutes the suspension from the front bubble and the particles flow out of the sample from the rear bubble. In that case, the average dilution of the sample is about 3%.
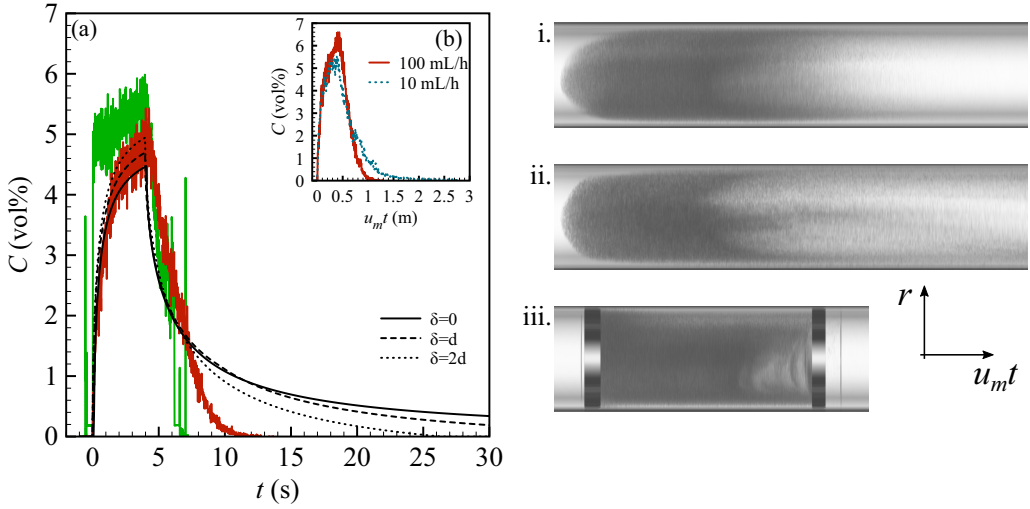
FIG. 4. (a) Time evolution of the volume fraction of a polystyrene beads suspension, having a diameter d of $20\,\mu$m, undergoing a convective dispersion at a flow rate of 100 mL/h in a capillary having a radius of $415\,\mu$m (red curve) and when two large bubbles bound the sample (green curve). The volume fraction is measured at $L_i = 10$ cm. The evolution predicted by Eq. (2) with various thicknesses δ of a depletion layer near the wall is also shown. The initial concentration C_0 is 5 vol%. (b) Dispersion curves for two different flow rates with C_0 equal to 6 vol%. The time is multiplied by the maximum velocity u_m. Corresponding spatiotemporal diagrams built along the transverse plane of the capillary for (i) $q = 100$ mL/h, (ii) $q = 10$ mL/h, and when bubbles are present at (iii) $q = 100$ mL/h. Time is also multiplied by u_m.

C. Convective dispersion of microparticles

We now wonder how larger particles behave in such a flow configuration. The time evolution of the concentration C of a suspension of micrometer beads injected in the same condition as in the experiment reported in Fig. 3(a) is shown in Fig. 4(a). The time evolution of C predicted by Eq. (2) is also shown. Like for a CNT suspension, after reaching a maximum, the concentration of beads decreases faster than predicted. However, the difference is more pronounced since particles are swept out in less than 15 s for beads, while traces of CNT are still present after 30 s. When the flow rate is divided by 10, the concentration decreases again less rapidly, but the maximum value reached by C is different [Fig. 4(b)]. For the highest flow rate, the maximal concentration is even larger than the sample one, C_0.

The fact that the concentration of beads decreases faster to zero than CNT is the signature of lateral migration experienced by the beads. Indeed, the fast concentration drop can be associated with a depletion of particles near the wall that do not explore low velocities responsible for the slow decay of C. The thickness of this depletion layer has been experimentally shown to be a decreasing function of the initial particle concentration [18]. Also, the concentration profile is evolving with time since particles migrate radially to reach a steady state that depends on the bulk concentration and the channel Reynolds number [19–21]. In order to simply illustrate the impact of the depletion layer, let us assume that there exists a layer near the wall of thickness δ depleted in particles and that the concentration of particles is then uniform, i.e., $\phi = 0$ for $r > a - \delta$ and $\phi = (r_f - r_b)/(a - \delta)$ for $r \leqslant a - \delta$. The bulk concentration C_0 is multiplied by $[1/(1 - \delta/a)]^2$ to conserve mass. As reported in Fig. 4(a), Eq. (2) results in a trend similar to experiments when ϕ and C are modified in such a way. In that case, the time t_0 at which the concentration is null is $t_0 = (L_i + L_s)/\{[1 - (1 - \delta/a)^2]u_m\}$, which tends to infinity when δ tends to 0. However, in the case of particles having a finite size, the depletion layer thickness is at least equal to $d/2$ due to steric hindrance.
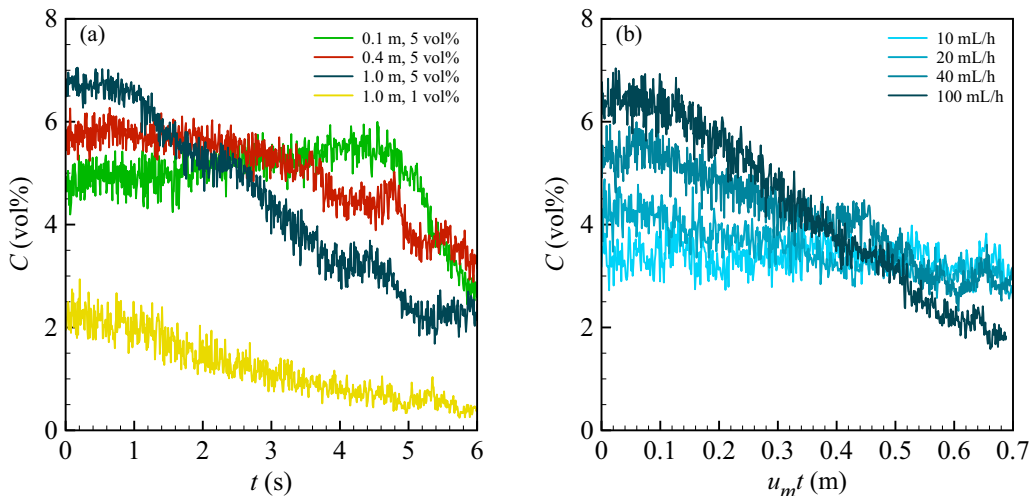
FIG. 5. (a) Time evolution of the concentration of a suspension of micrometer beads bounded by two large bubbles measured at three downstream distances L_i and for two initial concentrations C_0. The flow rate is set to 100 mL/h. (b) Influence of the flow rate on the distribution of beads initially homogeneously dispersed at $C_0 = 4$ vol% and sandwiched between two bubbles. The volume fraction is measured at $L_i = 1$ m. For comparing different flow rates, time is multiplied by the maximum velocity u_m. (b) Dimensionless gradient of the concentration as a function of the sample length L_s for two flow rates ($d = 20$ μm, $C_0 = 4$ vol%, $L_i = 1$ m).

D. Convective dispersion of microparticles with bubbles

As shown in Fig. 4(a), the distribution of beads when the sample is bounded by two long bubbles does not behave the same as for nanoparticles. The concentration starts at C_0, increases to about 5.8 vol%, and then decreases as it does without any bubble at the rear. What does happen if the measurement location is moved further downstream? The time evolution of C, for a sample initially at a homogeneous concentration of 5 vol% flowing at a flow rate of 100 mL/h, is reported in Fig. 5(a) for L_i equal to 0.1, 0.4, and 1.0 m. One can clearly see an accumulation of particles at the rear of the front bubble that increases with L_i. There exists a peak of concentration that propagates towards the front bubble and reaches here about 7 vol%. While the initial concentration is moderate, collision between particles is frequent. These collisions are known to induce a lateral migration, even at low Reynolds number [22]. However, when C_0 is set to 1 vol%, the accumulation feature is still present and the maximum reached by C is even twice C_0. The lift force experienced by the beads at such Reynolds number, $\mathrm{Re}_c = 76$, is high enough to promote a reorganization of the beads in the transverse plan that impacts their dispersion in the longitudinal direction. We mention that a companion Reynolds number, $\mathrm{Re}_p = \mathrm{Re}_c \times (d/4a)^2$, is usually introduced in such a context [23]. The corresponding particle Reynolds number is equal to $\mathrm{Re}_p = 0.012$. If now the flow rate is divided by 10, and thus Re_p, this phenomenon is barely visible [Fig. 5(b)]. Then, the accumulation of particles is more pronounced when the flow rate increases.

In order to define a general trend of the suspension behavior under flow, one can estimate a gradient of the concentration dC/dx, where $x = u_m t$. The gradient as a function of the flow rate q is reported in Fig. 6(a) (●). Since the migration dynamics of particles depends on the particle Reynolds number, let us examine how the size of particles and tube as well as the viscosity of the continuous phase impact the flow feature of the suspensions. For a larger tube size [Fig. 6(a) (■)], dC/dx seems to grow less as a function of q. For larger particles [Fig. 6(a) (▲)], the accumulation phenomenon occurs at lower flow rates and the gradient of C grows rapidly with the flow rate. On the other hand, the suspension becomes heterogeneous for larger critical flow rates for more viscous continuous phases [Fig. 6(a) (▼, ♦)]. The growth of dC/dx with q is a decreasing function of the
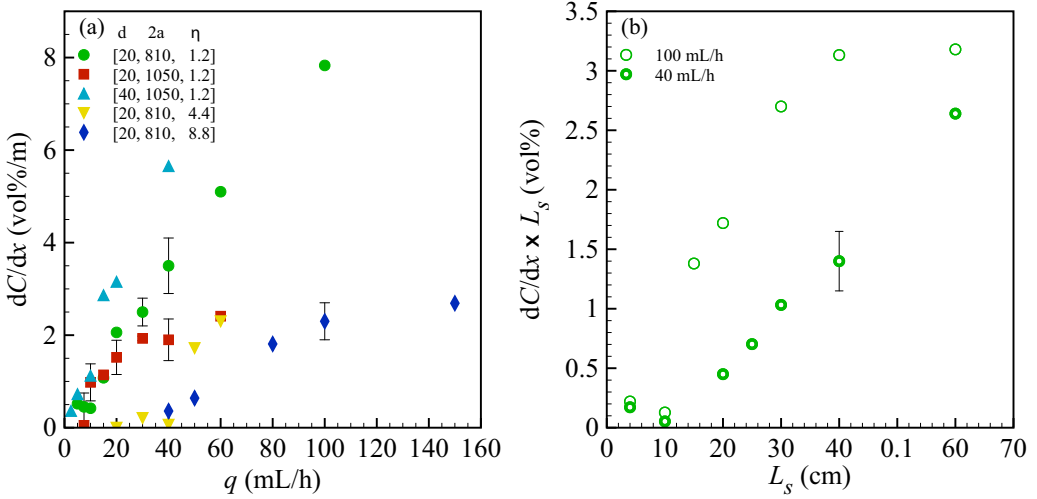
FIG. 6. (a) Gradient of the concentration measured at $L_i = 1$ m as a function of the flow rate for various beads and tube sizes as well as liquid viscosities for $C_0 = 4$ vol%. The corresponding beads diameter d, tube diameter $2a$, and dynamic viscosity η are indicated in μm and mPa s, respectively. (b) Dimensionless gradient of the concentration as a function of the sample size for two flow rates ($d = 20$ μm, $L_i = 1$ m, $C_0 = 4$ vol%).

viscosity η. The error on the evaluation of the gradient for multiple experiments, between 2 and 4, is rather high, of the order of 20%. This is probably due to slight sedimentation of the particles during the experiment.

We now wonder how the length of this recirculating flow cell impacts the spatial distribution of particles. The sample length L_s is thus varied from 4 to 60 cm. The concentration C is assessed at a distance $L_i = 1$ m for two flow rates, 40 and 100 mL/h. The average variation of concentration from one bubble to the other one, i.e., $dC/dx \times L_s$, is reported in Fig. 8(a) as a function of L_s. We note that the sample remains homogeneous for L_s up to 10 cm. Then, accumulation of particles behind the bubble moving in front takes place. The variation of C is more pronounced for the largest flow rate, in accordance with an enhanced inertial migration (Fig. 5), and increases with L_s.

As previously discussed, a depletion layer of particles near the wall reduces the overall dispersion of a suspension [Fig. 4(a)]. In order to illustrate its effect in the case of an axially confined flow, let us follow the same simple model where $\phi = 0$ for $r > a - \delta$ and $\phi = 1$ for $r \leqslant a - \delta$. The long bubbles travel at velocity $u_b = (1 + \alpha)U$, where the slip coefficient α is of the order of $(\eta U/\gamma)^{2/3}$ [17]. Here, the capillary number Ca $= \eta U/\gamma$ is at most equal to 10^{-3}, corresponding to a bubble velocity u_b that is 3% larger than the average fluid velocity U. In the reference frame of the bubble, the fluid velocity is

$$u'(r) = u_m \left[\frac{1 - \alpha}{2} - \left(\frac{r}{a} \right)^2 \right]. \tag{3}$$

This flow profile is valid at a distance from the bubble of the order of the tube's radius a, as illustrated in Fig. 7(a). By assuming that particles travel at the local fluid velocity, the density flux of particles is $j = C_0' \phi(r) u'(r)$, where $C_0' = C_0[1/(1 - \delta/a)]^2$. The flux of particles passing through the cross section of the pipe is then

$$J = 2\pi \int_0^{a-\delta} j(r) r \, dr$$

$$= \frac{\pi}{2} a^2 C_0 \left(\frac{1}{1 - \delta/a} \right)^2 \left[(1 - \alpha) \left(1 - \frac{\delta}{a} \right)^2 - \left(1 - \frac{\delta}{a} \right)^4 \right]. \tag{4}$$
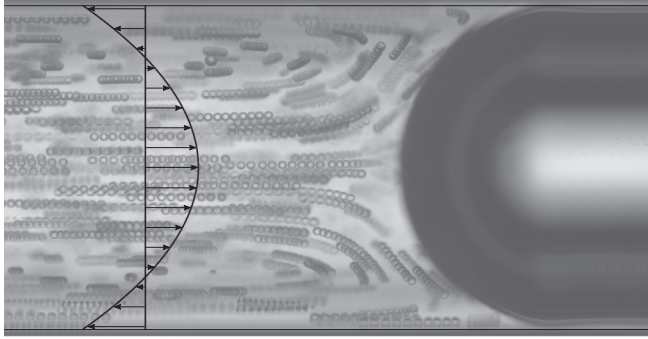
FIG. 7. Trajectories of beads at the rear of the front bubble in the reference frame of the latter ($C_0 = 0.5$ vol%, $d = 20$ μm, $2a = 810$ μm, q=100 mL/h). The image is a superposition of 10 snapshots with a time interval of 0.5 ms. The velocity field is also shown.

There is therefore a net flux of particles directed towards the front bubble if $\delta/a > 1 - (1 - \alpha)^{1/2}$. When $\delta = 0$, such as in the experiment with a carbon nanotube suspension, the flux becomes negative since the bubbles always travel faster than the average liquid velocity. Since CNT can flow through the lubricating film, particles are left behind the rear bubble and the suspension is diluted from the front bubble [Fig. 3(a)]. For PS beads, since their size is larger than the lubricating film, only a few particles could escape [Fig. 4(a)], maybe due to a mechanism recently discussed where particles adhere to the interface [24].

However, particles are principally trapped between the two bubbles and the proper boundary condition of the flux should be set at each liquid-air interface in order to assess the flow feature of such a bounded suspension. As observed in Fig. 7, in the reference frame of the bubble, particles are moving towards the bubble apex at the center and flow back close to the wall. Since the capillary number lies between 10^{-4} to 10^{-2}, leading thus to a thin lubricating film with a maximum thickness of about 5 μm [17], closed streamlines are indeed expected to occur [25,26]. At the rear bubble, the low volume fraction region from the wall invades the core. On the other side, at the front bubble location, the high volume fraction of the core refills the near wall region. There is therefore a competition between the homogenization due to the recirculating flow and the lateral migration of particles due to liquid inertia.

Mixing efficiency should depend on the sample length L_s as it sets the recirculation time τ_r required for a volume of fluid to be transported from one bubble to the other one. The region of the suspension that flows towards the front bubble, defining the core of the toroidal vortex, is located between the tube's center and the radius r_0, where the velocity is equal to the bubble's velocity, i.e.,

$$r_0 = a\left(\frac{1 - \alpha}{2}\right)^{1/2}. \tag{5}$$

The corresponding average velocity u_0 is

$$u_0 = \frac{2}{r_0^2} \int_0^{r_0} u'(r)r dr = \frac{(1 - \alpha)}{4} u_m. \tag{6}$$

The recirculation time is simply $\tau_r = L_s/u_0$. Lateral migration then occurs if the transversal migration velocity v_m is fast enough to reorganize particle distribution. The migration velocity scales as $v_m \sim u_m \text{Re}_p (d/2a)$ and it is a function of the radial location [23]. However, one can make a rough estimate of the displacement made during τ_r and compare it to the tube radius a, i.e.,

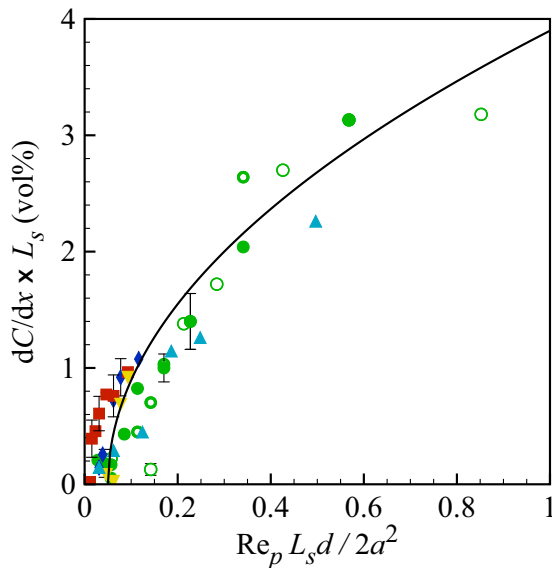$$\frac{v_m \tau_r}{a} \sim \text{Re}_p \frac{L_s d}{2a^2}. \tag{7}$$

FIG. 8. Dimensionless gradient of the concentration as a function of the particle Reynolds number times the sample length and particle size normalized by the tube radius for the same conditions as in Fig. 6. The continuous line is a critical function (see text for details). We note that the injection length L_i here is always larger than the sample length L_s.

Once the dimensionless gradient is plotted as a function of the normalized recirculation time given by Eq. (7), the data tend to collapse on a single master curve (Fig. 8). One can even fit a critical function, i.e., $dC/dx \times L_s \sim (y - y_c)^{0.5}$ where $y = \mathrm{Re}_p L_s d/2a^2$. The data are too scattered to clearly identify a bifurcation, but the experiments give an estimate of a particle Reynolds times the sample length and particle size normalized by the tube radius above which heterogeneities of the suspension under flow appear, which is $(\mathrm{Re}_p L_s d/2a^2)^* = (5 \pm 2) \times 10^{-2}$.

The present experiments give an overview of the features of such a multiphasic flow, but it is necessary to correctly describe the lateral flux of particles due to inertial migration in order to predict the accumulation dynamics.

IV. CONCLUSION

In this work, we report an experimental investigation of flowing suspensions in a pipe, sandwiched or not by two long confined bubbles. Here, the suspensions are dilute and flow at moderate Reynolds numbers for which liquid inertia affects the motion of particles that migrate away from the wall. When a finite volume of the suspension is injected in the flow of the continuous phase free of particles, we observe that particle migration has a strong impact on the distribution of particles undergoing convective dispersion. Indeed, particles are swept away faster because of the existence of a depletion layer of particles at the wall that do not explore low velocities otherwise responsible for a slow decay of particle concentration distribution. If now the sample is bounded by two long bubbles, particles tend to accumulate behind the front bubble. This phenomenon is shown to occur above a critical particle Reynolds number times the sample length and particle size normalized by the tube radius, $(\mathrm{Re}_p L_s d/2a^2)^* = (5 \pm 2) \times 10^{-2}$.

All of the results are rationalized with the help of a minimal model that accounts for the presence of a depletion layer near the wall, but with a homogeneous concentration of particles in the outer region. A more sophisticated model is then required for describing the dynamics of the

destabilization of the initially homogeneous suspension that would account for the establishment of particle accumulation at the rear bubble linked to a redistribution of particles in the radial direction.

The phenomenon of particle accumulation in such a multiphase flow is shown here to occur when liquid inertia comes into play, but we believe that it is more generic. Indeed, a criterion to satisfy is the establishment of a layer near the wall depleted in particles, as is observed for the flow of concentrated suspensions at low Reynolds numbers or in the case where particles are deformable, as for biological samples or emulsions [2].

[1] L. Leal, Particle motions in a viscous fluid, Ann. Rev. Fluid Mech. **12**, 435 (1980).

[2] A. Kumar and M. D. Graham, Margination and segregation in confined flows of blood and other multicomponent suspensions, Soft Matter **8**, 10536 (2012).

[3] G. Segré and A. Silberberg, Behaviour of macroscopic rigid spheres in Poiseuille flow part 2. Experimental results and interpretation, J. Fluid Mech. **14**, 136 (1962).

[4] D. Di Carlo, Inertial microfluidics, Lab. Chip **9**, 3038 (2009).

[5] J.-P. Matas, V. Glezer, É. Guazzelli, and J. F. Morris, Trains of particles in finite-Reynolds-number pipe flow, Phys. Fluids **16**, 4192 (2004).

[6] J. F. Edd, D. Di Carlo, K. J. Humphry, S. Köster, D. Irimia, D. A. Weitz, and M. Toner, Controlled encapsulation of single-cells into monodisperse picolitre drops, Lab. Chip **8**, 1262 (2008).

[7] U. Prusse, L. Bilancetti, M. Bucko, B. Bugarski, J. Bukowski, P. Gemeiner, D. Lewinska, V. Manojlovic, B. Massart, C. Nastruzzi *et al.*, Comparison of different technologies for alginate beads production, Chem. Pap. **62**, 364 (2008).

[8] H. Domejean, M. de la Motte Saint Pierre, A. Funfak, N. Atrux-Tallau, K. Alessandri, P. Nassoy, J. Bibette, and N. Bremond, Controlled production of sub-millimeter liquid core hydrogel capsules for parallelized 3d cell culture, Lab. Chip **17**, 110 (2017).

[9] H. Doméjean, J. Bibette, and N. Bremond, Traffic collision during the breakup of an aqueous viscous compound jet, Phys. Rev. Fluids **1**, 063903 (2016).

[10] G. I. Taylor, Dispersion of soluble matter in solvent flowing slowly through a tube, Proc. R. Soc. London A **219**, 186 (1953).

[11] M. T. Kreutzer, F. Kapteijn, J. A. Moulijn, and J. J. Heiszwolf, Multiphase monolith reactors: Chemical reaction engineering of segmented flow in microchannels, Chem. Eng. Sci. **60**, 5895 (2005).

[12] A. Günther, S. A. Khan, M. Thalmann, F. Trachsel, and K. F. Jensen, Transport and reaction in microscale segmented gas–liquid flow, Lab. Chip **4**, 278 (2004).

[13] A.-K. Liedtke, F. Bornette, R. Philippe, and C. de Bellefon, External liquid solid mass transfer for solid particles transported in a milli-channel within a gas–liquid segmented flow, Chem. Eng. J. **287**, 92 (2016).

[14] L. Mottet, D. Le Cornec, J.-M. Noël, F. Kanoufi, B. Delord, P. Poulin, J. Bibette, and N. Bremond, A conductive hydrogel based on alginate and carbon nanotubes for probing microbial electroactivity, Soft Matter **14**, 1434 (2018).

[15] R. Aris, On the dispersion of a solute in a fluid flowing through a tube, Proc. R. Soc. London A **235**, 67 (1956).

[16] S. A. Berger, L. Talbot, and L. S. Yao, Flow in curved pipes, Ann. Rev. Fluid Mech. **15**, 461 (1983).

[17] F. P. Bretherton, The motion of long bubbles in tubes, J. Fluid Mech. **10**, 166 (1961).

[18] A. Karnis, H. L. Goldsmith, and S. G. Mason, The flow of suspensions through tubes: V. inertial effects, Can. J. Chem. Eng. **44**, 181 (1966).

[19] C. J. Koh, P. Hookham, and L. G. Leal, An experimental investigation of concentrated suspension flows in a rectangular channel, J. Fluid Mech. **266**, 1 (1994).

[20] P. R. Nott and J. F. Brady, Pressure-driven flow of suspensions: Simulation and theory, J. Fluid Mech. **275**, 157 (1994).

[21] M. K. Lyon and L. G. Leal, An experimental study of the motion of concentrated suspensions in two-dimensional channel flow. Part 1. Monodisperse systems, J. Fluid Mech. **363**, 25 (1998).

[22] F. R. Da Cunha and E. J. Hinch, Shear-induced dispersion in a dilute suspension of rough spheres, J. Fluid Mech. **309**, 211 (1996).

[23] B. Ho and L. Leal, Inertial migration of rigid spheres in two-dimensional unidirectional flows, J. Fluid Mech. **65**, 365 (1974).

[24] Y. E. Yu, S. Khodaparast, and H. A. Stone, Armoring confined bubbles in the flow of colloidal suspensions, Soft Matter **13**, 2857 (2017).

[25] G. I. Taylor, Deposition of a viscous fluid on the wall of a tube, J. Fluid Mech. **10**, 161 (1961).

[26] T. C. Thulasidas, M. A. Abraham, and R. L. Cerro, Flow patterns in liquid slugs during bubble-train flow inside capillaries, Chem. Eng. Sci. **52**, 2947 (1997).